26 August 2024

Indirect Constraints of the Charm-Yukawa Interaction by Analysing Higgs Boson Production through the $H \to \gamma\gamma$ ATLAS Measurements

Sienna Lam Chi-yin

Summary

I worked with Dr. Petar Bokan and Dr. Valentina Cairo to interpret the Higgs boson differential cross-section in the $H \to \gamma\gamma$ final state to set an indirect constraint on the interactions between Higgs bosons and Charm quarks. We analysed the effect of dependence of the Higgs boson production on the Charm-Yukawa interaction coupling strength. The Higgs boson production cross-section is parameterised in terms of the Charm-Yukawa, Bottom-Yukawa and Top-Yukawa coupling strength modifiers. They are then constrained by fitting the parameterisation to the Higgs boson differential cross-section as a function of the Higgs boson transverse momentum, in the $H \to \gamma\gamma$ final state as measured by the ATLAS experiment

ATLAS Doc:	xxx-yyy-zzzz	
EDMS Id:	123456	
Version:	0.1	
Last modified:	`08:03 on 26 August 2024`	
Prepared by: S. Lam	**Checked by:** P. Bokan	**Approved by:** V. Cairo

Contents

1 Introduction **4**

2 Charm-Yukawa Coupling **5**

3 Statistical Analysis **8**

3.1 Merged Parameterisation 10

4 Conclusions **15**

List of Figures

1 ATLAS has consists of 4 detectors: Inner Tracker, Electromagnetic Calorimeter, Hadronic Calorimeter and Muon Spectrometer. Bianchi and ATLAS [2022] 4

2 Higgs boson must produce a loop of massive particles, such as the W boson or heavy quarks, in order to decay into 2 photons. ATLAS [2022] 5

3 Gluon-gluon Fusion process, where the fermion propagators are either Top, Bottom or Charm quarks. Because the initial and final states of gluon-gluon Fusion are the same, different quark flavours can interfere ATLAS [2022]. . 7

4 Higgs boson decays into a quark-antiquark pair, which could be either Bottom or Charm quarks. The diagram can also be read from right to left, as the fusion of a quark-antiquark pair to produce a Higgs boson ATLAS [2022]. 7

5 Differential cross-section of the Higgs boson production modes. ggF refers to Gluon-Gluon Fusion, qqF refers to Quark-Quark Fusion, ttH is $gg \to ttH$, VBF is Vector Boson Fusion $qq \to VV \to H$, and VH is direct Higgs Boson production from a single Vector boson as follows $qq \to V \to VH$. . . 7

6 Piechart showing the relative contribution of each production mode to the Higgs boson production, including interference terms in Gluon-Gluon Fusion. The legend is sorted from smallest to largest in terms of absolute value of the contributions to the cross-section, which was also used to sort the legend for Figure 5. 8

7 Change in the differential cross-section for a few different parameters as indicated in the legend 9

8 The κ_c NLL scan, where all other parameters of interest are freely floated while minimising the Negative Logarithm Likelihood. There are actually 2 minimums but they overlap. 11

9 The κ_b NLL scan, where all other parameters of interest are freely floated while minimising the Negative Logarithm Likelihood. There are 2 minimums as the model is quadratic in κ_b. 11

10 The κ_t NLL scan, where all other parameters of interest are freely floated while minimising the Negative Logarithm Likelihood.The constraints are stronger as the cross-sectional terms for the Top-Yukawa interaction are larger than those of the Bottom-Yukawa and Charm-Yukawa interactions. . 12
11 Impact Rankings for κ_b, nominal parameterisation 13
12 Impact Rankings for κ_b, merged parameterisation 13
13 Negative-Log Likelihood scan for κ_b using Asimov data. 14
14 Negative-Log Likelihood scan for κ_b using Asimov data. Notice that there are 2 tiny minima right next to each other, because these minima are a relic of the quadratic terms in the parameterised model. 14
15 Negative-Log Likelihood scan for κ_t using Asimov data. Because the measured data for κ_t has a stronger constraint than the others and is known to be close to 1, that's why the minimum is around 1. 15

List of Tables

1 Introduction

The LHC, short for Large Hadron Collider, is a synchrotron which has a radius of 27 kilometers and a centre-of-mass energy of 13.6 TeV. It collides hadrons such as protons or ions in specific interaction points so that the collision products can be detected by various experiments, including ATLAS, ALICE, LHCb and CMS.

ATLAS, short for A Toroidal LHC Apparatus, is a general-purpose detector that along with CMS, studies phenomena of elementary particles predicted by the Standard Model, and it looks for particles beyond the Standard Model at the large energy scales. It is the largest experiment analysing the collisions in the LHC. The structure of ATLAS is shown in Figure 1. The z-axis is defined along the beam axis in the longitudinal direction, because the conservation laws cannot be used for longitudinal momentum as the initial proton energy fractions that interact in the collision are not known. Therefore, the transverse momentum as projected into the x and y axes is used, so that it follows the momentum and energy conservation laws.

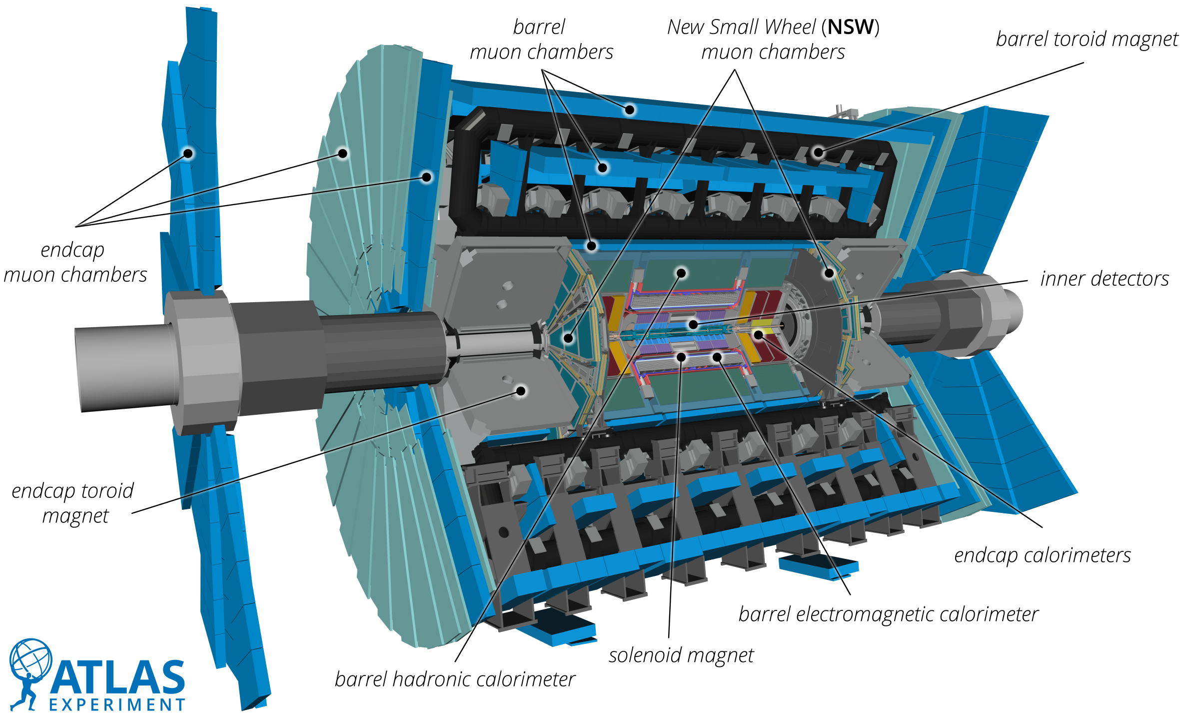

Figure 1: ATLAS has consists of 4 detectors: Inner Tracker, Electromagnetic Calorimeter, Hadronic Calorimeter and Muon Spectrometer. Bianchi and ATLAS [2022]

The first detector in ATLAS is the inner tracker which contains silicon pixel detectors and strip detectors (also known as semiconductor tracker) and transition radiation tracker. It detects the positions of charged particles as they pass through layers of pixels. There is also a magnet which bends the charged particle trajectory in a into a helical that is proportional to the particle momentum and charge.

Photons and electrons are detected in the Electromagnetic calorimeter which uses a

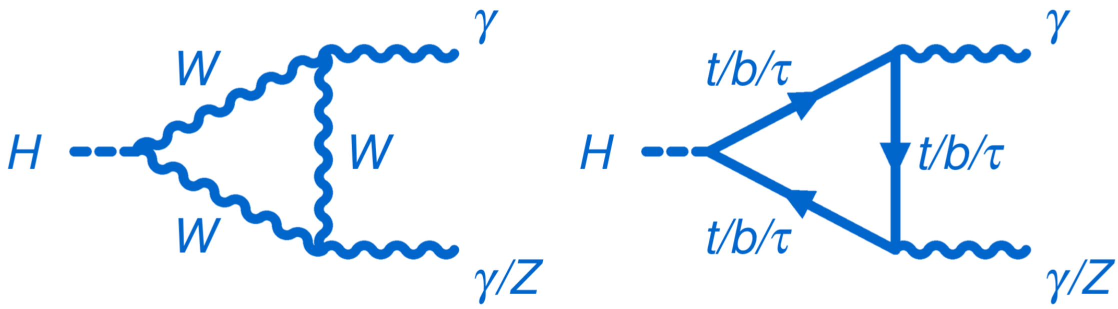

Figure 2: Higgs boson must produce a loop of massive particles, such as the W boson or heavy quarks, in order to decay into 2 photons. ATLAS [2022]

Liquid Argon scintillator to measure their energy. Photons can only be detected with this calorimeter because they are not charged so they do not interact with the inner tracker. The calorimeter contains lead absorbers and electrodes, held in place by a honeycomb structure. Each honeycomb section contains Liquid Argon as the active layer of the calorimeter. Wilkens and ATLAS [2009] When a photon or an electron collides with the lead, it undergoes an electromagnetic shower by decaying into positron-electron-pairs or emitting photons respectively, causing an electromagnetic shower. The final products of the shower ionise the Argon to produce a measurable current that is proportional to the energy of the initial particle.

There is also a Hadronic Calorimeter which detects the energy of hadrons, using many plates of plastic scintillators. Hadrons will undergo hadronic showers in a manner analogous to electromagnetic showers, creating measurable clusters of energy in the scintillators which are proportional to the energy of the initial hadron.

The last component is the Muon Spectrometer which has a large toroidal magnet to bend the trajectory of the muons so that the momentum can be determined from the curvature of the trajectory. The Muon Spectrometer is very large to increase the momentum resolution by allowing the magnets to bend the trajectory to a greater degree.

Photons can be detected with high resolution using the electromagnetic calorimeter because they have a clean final state. This is why the Higgs boson was first detected from $H \to \gamma\gamma$ production, even though they only have a branching ratio of 0.223% pb ATLAS [2022]. The reason that the branching ratio is low is because photons have no mass, so they only couple to the Higgs boson through production of an intermediary massive particle as shown in Figure 2.

2 Charm-Yukawa Coupling

The Higgs field is a scalar field which has a non-zero value in the vacuum. Excitations of this field will create Higgs boson particles with a mass of 125.09 GeV ATLAS [2023a] that can interact directly with all massive particles.

The Standard Model predicts that interactions between fermions and the Higgs boson are proportional to the fermion's mass, but for interactions between the Higgs boson and other bosons it is proportional to the square of the boson's mass.

The coupling strength for the Top-Yukawa, Bottom-Yukawa and Tau-Yukawa interactions have been precisely determined, but the Charm-Yukawa interaction is quite hard to measure. Currently, direct measurements of $H \to c\bar{c}$ only yield a constraint on the coupling modifier of $|\kappa_c| < 4.2$ ATLAS [2024], where $\kappa_c = \frac{y_c}{y_c^{SM}}$ where y_c is the coupling strength. One of the reasons is because the $H \to c\bar{c}$ decay is rare, because the charm quark is very light at only 1.27 GeV. This causes the $H \to c\bar{c}$ to have a branching ratio of around 2.884% ATLAS [2022] as calculated in the Standard Model. In addition, Charm-quark-initiated jets are difficult to distinguish from other quark or gluon jets. Charm quarks are also produced in many other processes when 2 protons are collided, such as the $Z \to c\bar{c}$ decay, which means that the background rates for $H \to c\bar{c}$ are very high.

As an alternative, indirect detection method can be used, by measuring the effect of the Charm-Yukawa interaction on Higgs boson production. The Charm-Yukawa interaction affects Higgs boson production because some of the production modes directly depend on it, with the cross-section given by the Equation 1. In this equation, the Standard Model predicted cross-sections for all major production modes are scaled by multiplying them directly with the coupling modifiers if they depend on Charm-Yukawa, Bottom-Yukawa and Top-Yukawa interactions respectively Bokan et al. [2022]:

$$\sigma_{pp\to H} = \kappa_t^2(\sigma_{ggF}^{tt} + \sigma_{ttH}) + \kappa_t\kappa_b\sigma_{ggF}^{tb} + \kappa_c\kappa_t\sigma_{ggF}^{ct} + \kappa_b\kappa_c\sigma_{ggF}^{bc} + \kappa_b^2(\sigma_{ggF}^{b} + \sigma_{b\bar{b}\to H}) + \kappa_t^2(\sigma_{ggF}^{t} + \sigma_{t\bar{t}\to H}) + \sigma_{other} \quad (1)$$

The Charm quark is involved in Higgs boson production in 2 ways. The first is gluon-gluon Fusion, where 2 gluons form a loop of Charm Quarks which allows them to combine into the Higgs boson, as shown in Figure 3. The loop of charm quarks also interferes with the loops of Top and Bottom quarks, overall having a combined impact on the Higgs boson production cross-section.

The second is Quark-Quark Fusion, where a Charm quark and a Charm antiquark annihilate to produce a Higgs boson, as shown in Figure 4. This requires the two particles to have a total centre-of-mass energy greater than the Higgs boson mass-energy of 125.09 GeV.

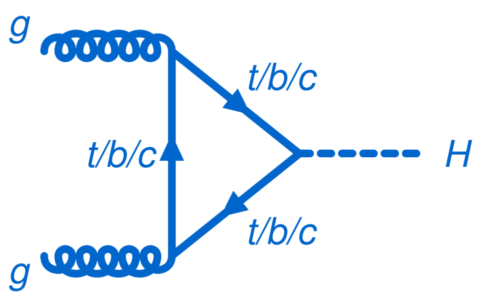

Figure 3: Gluon-gluon Fusion process, where the fermion propagators are either Top, Bottom or Charm quarks. Because the initial and final states of gluon-gluon Fusion are the same, different quark flavours can interfere ATLAS [2022].

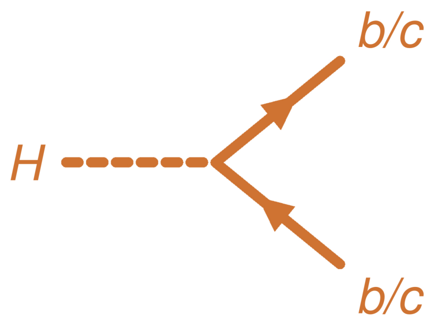

Figure 4: Higgs boson decays into a quark-antiquark pair, which could be either Bottom or Charm quarks. The diagram can also be read from right to left, as the fusion of a quark-antiquark pair to produce a Higgs boson ATLAS [2022].

The Standard Model predicts the contributions of each term for the parameterised cross-section given in Equation 1. Using the predicted SM values for the contributions to the differential cross-section as a function of Higgs boson transverse momentum, and then dividing the cross-sections by the momentum width of each bin, we can produce a graph that shows the contribution of each term to the total differential cross-section, as shown in Figure 5:

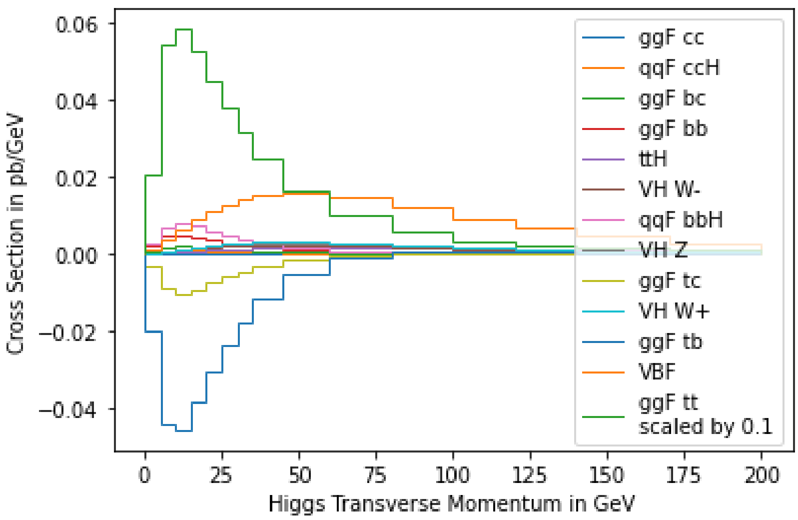

Figure 5: Differential cross-section of the Higgs boson production modes. ggF refers to Gluon-Gluon Fusion, qqF refers to Quark-Quark Fusion, ttH is $gg \to ttH$, VBF is Vector Boson Fusion $qq \to VV \to H$, and VH is direct Higgs Boson production from a single Vector boson as follows $qq \to V \to VH$.

As the graph shows, the Top-Top gluon-gluon fusion term has the largest contribution

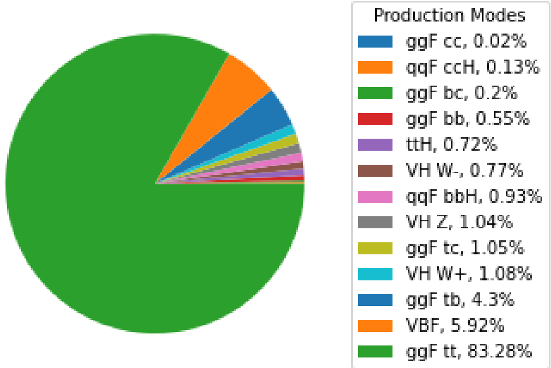

Figure 6: Piechart showing the relative contribution of each production mode to the Higgs boson production, including interference terms in Gluon-Gluon Fusion. The legend is sorted from smallest to largest in terms of absolute value of the contributions to the cross-section, which was also used to sort the legend for Figure 5.

by far, so it is scaled by a factor of 0.1 to make the other contributions more visible. This is because Top quark mass (172.52 ± 0.33 GeV) CMS and ATLAS [2024] is larger than Bottom quark mass ($4.18^{0.03}_{-0.02}$ GeV) Workman et al. [2022] and Charm quark mass (1.27 ± 0.02 GeV) Workman et al. [2022], so the top quarks couple most strongly to the Higgs boson.

The terms can be sorted by their contribution to the cross-section, using the Riemann sum of the step-like curves, to find the area under each curve. This reveals the predominance of Top-Top Gluon-Gluon Fusion, Vector boson Fusion and Top-Bottom Gluon-Gluon Fusion interference over all other terms, as shown in Figure 6.

Visualising the effect of varying the κ_c and κ_b coupling modifiers on the Higgs boson production cross-section, the predicted differential cross-sections for a predefined set of transverse momentum bins was plotted using the post-fit parameterised model. As shown in Figure 7, it becomes clear that when increasing κ_c or κ_b, the peak of the Higgs boson production differential cross-section increases, while the shape remains similar. However, when κ_c or κ_b are negative, the shape of the differential cross-section changes because the cross-section in the higher momentum bins is suppressed while the cross-section in the lower momentum bins is enhanced.

3 Statistical Analysis

A statistical analysis of the Higgs boson production differential cross-section ATLAS [2023b] can fit the parameters in Equation 1 to the ATLAS data. The fit is used to statistically infer the constraints on the coupling modifiers such as κ_c.

We use a multivariate Gaussian Likelihood, which takes the form of the Equation 2 as shown below:

$$L(\vec{\sigma}(\vec{\kappa}, \vec{\theta})|\vec{x}, \boldsymbol{V}) = e^{\left(-\frac{1}{2}(\vec{x}-\vec{\sigma})^T \boldsymbol{V}^{-1}(\vec{x}-\vec{\sigma})\right)} \times \prod_j \mathrm{Gauss}(\theta_j; 0, 1) \tag{2}$$

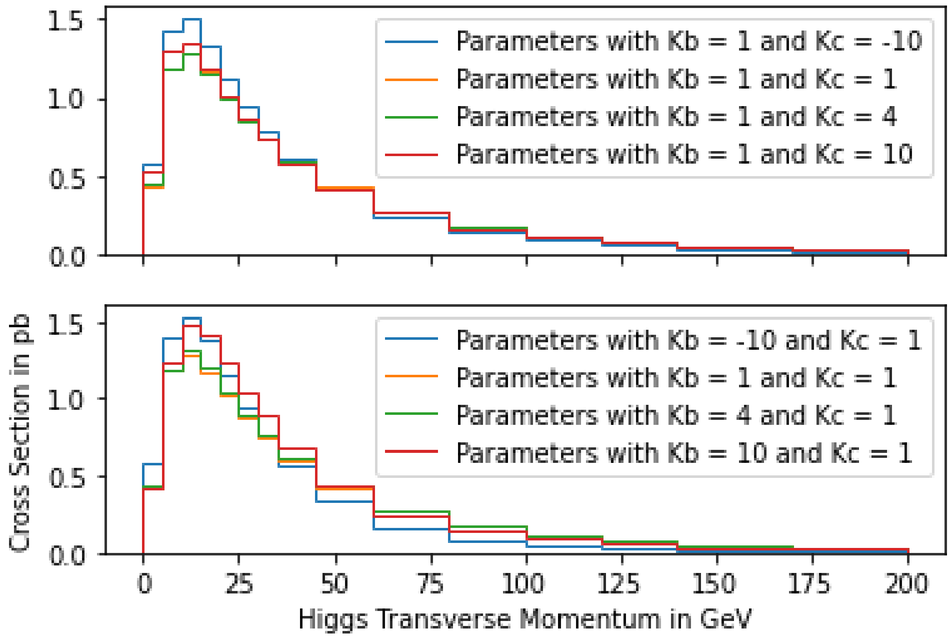

Figure 7: Change in the differential cross-section for a few different parameters as indicated in the legend

The vector $\vec{x}$ is a list of all of the ATLAS measurements in the form of a vector of all the Higgs boson cross-sections in the given momentum bin, and $\boldsymbol{V}$ is the covariant matrix of these measurements. $\vec{\sigma}$ is a vector of all the predicted cross-sections in a given momenntum bin, including as functions of the parameters of interest ($\vec{\kappa}$), and also as functions on the nuisance parameters ($\vec{\theta}$). The dependence on the parameters of interest, in this case the coupling modifiers, is shown in 1, while the dependence on the nuisance parameters is shown below in 3.

$$\sigma_{predicted} \rightarrow \sigma_{predicted}(1 + \theta\Delta\theta) \tag{3}$$

The Gauss($\theta_j; 0, 1$) term represents a constraint on the values of the nuisance parameter θ_j to make them follow a Gaussian probability distribution with the mean taken as 0 and the standard deviation taken as 1. In this context, the nuisance parameters represent the systematic uncertainties of the ATLAS experiment. These include the calculation and resummation uncertainties, QCD scale uncertainty, uncertainties in Parton Distribution Function and uncertainties in Parton Shower model ATLAS [2023b]. They modify the cross-section using the Equation 3:

$\Delta\theta$ is defined as the measured uncertainty of the ATLAS data in a given transverse momentum bin, while θ is the nuisance parameter that can be varied in the model.

The likelihood is maximised using an algorithm called Minuit2, which automatically varies the parameters until the function maximum is found. James and Winkler [2004]. This analysis only takes into account the shape of the Higgs boson differential cross-section to constrain the free parameters of the model, which is done by introducing a free normalisation parameter that affects all momentum bins in a correlated manner.

We can construct the likelihood ratio out of the conditional and unconditional maximum likelihoods. The conditional likelihood is defined as the likelihood function where all parameters are freely floating except for κ_c, while the unconditional likelihood also sets κ_c to be freely floating. Then, the likelihood ratio is constructed in the Equation 4 ATLAS [2022]:

$$\Lambda(k_c) = \frac{L_{conditional}(\hat{\hat{\vec{\kappa}}}, \hat{\hat{\vec{\theta}}}|\kappa_c = k_c)}{L_{unconditional}(\hat{\vec{\kappa}}, \hat{\vec{\theta}})} \tag{4}$$

After this, a test statistic can be made using the Equation 5 below. Test statistics measure the agreement between the model at a given value of κ_c to set the 68% and 95% confidence level intervals for the observed value of κ_c.

$$T = -2 \ln \Lambda(k_c) \tag{5}$$

Instead of maximising the likelihood, we can minimise the 'Negative Logarithm Likelihood' as defined in 5, for which the confidence levels of 68% and 95% correspond to the values of κ_c for which the Negative Logarithm Likelihood is either 1 or 3.84 greater than minimum respectively. On the following page, Figure 8, Figure 9 and Figure 10 are some 'Negative Logarithm Likelihood' scans. Taking 20 values of k_c, and then plotting them on the x-axis, versus the test statistic T on the y-axis, will produce a curve that will intersect with lines corresponding to 68% and 95% confidence levels. For κ_c and κ_b they are [-9.8, 11.5] and [-2.0, 8.1] for 68% confidence limit respectively. For the 95% confidence limit, they are [-14.4, 18.9] and [-3.7, 10.2] respectively. These confidence intervals are only based on the shape of the Higgs boson production cross-section as a function of the transverse momentum, and this is significantly less stringent than the more model-dependent scenario, where the total Higgs boson production cross-section is dependent on κ_b and κ_c.

3.1 Merged Parameterisation

To test a simpler parameterisation where the production modes independent of κ_c, κ_b and κ_t are merged, the cross-sections for them are combined. For the cross-sectional terms that are merged in the new parameterisation, the modal predicted cross-sections are summed. Systematical uncertainties are assumed to be uncorrelated, so they must be summed using the quadrature in each bin independently, as given in Equation 6. The overall effect of the merging procedure is to weaken the constraints on the parameters by a small amount. For instance, the 95% confidence limits for κ_c became [-14.5, 18.8] while for κ_b, they became [-3.8, 10.3].

$$\Delta x = \sqrt{(\Delta x_1)^2 + (\Delta x_2)^2 + \ldots + (\Delta x_n)^2} \tag{6}$$

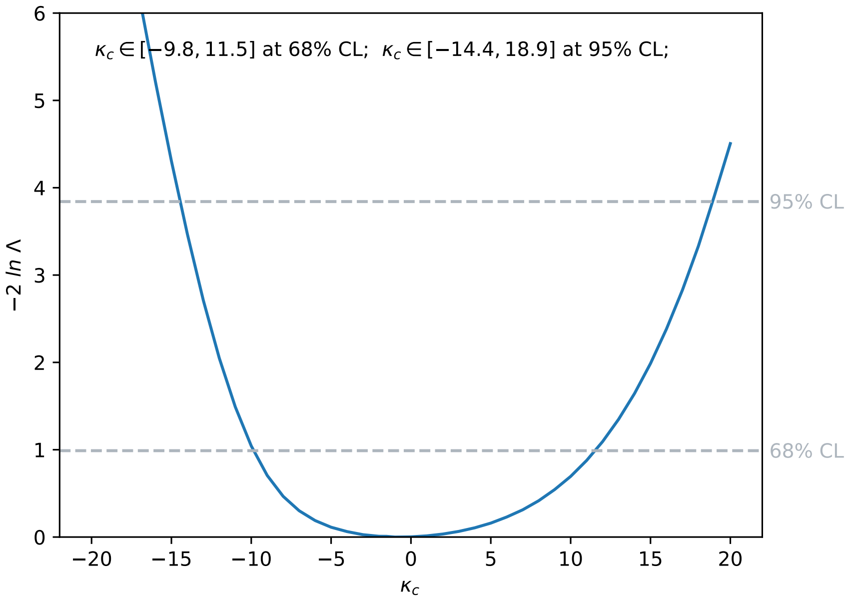

Figure 8: The κ_c NLL scan, where all other parameters of interest are freely floated while minimising the Negative Logarithm Likelihood. There are actually 2 minimums but they overlap.

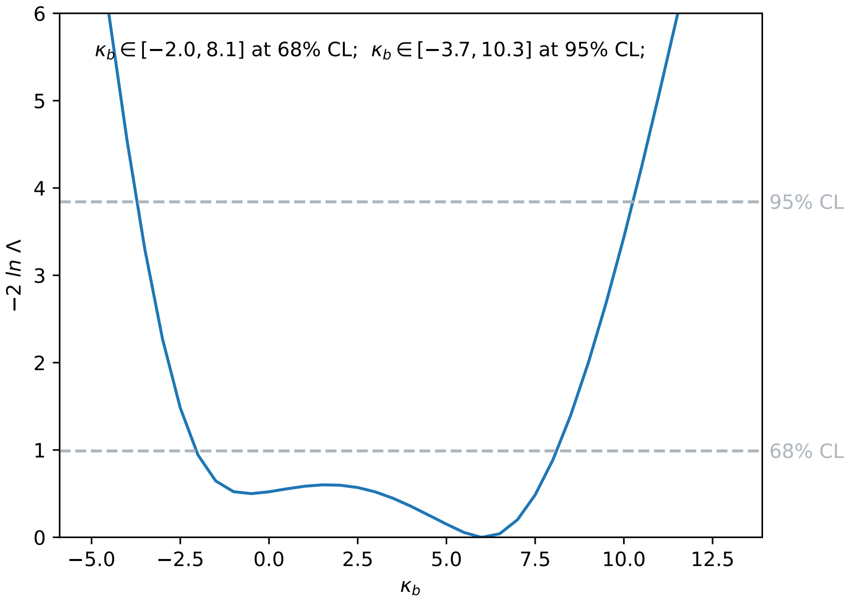

Figure 9: The κ_b NLL scan, where all other parameters of interest are freely floated while minimising the Negative Logarithm Likelihood. There are 2 minimums as the model is quadratic in κ_b.

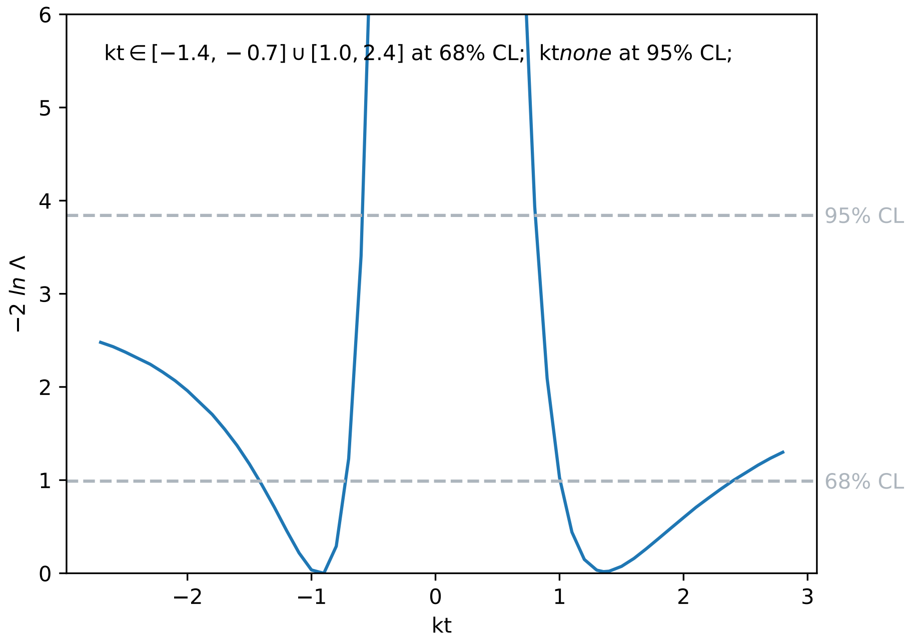

Figure 10: The κ_t NLL scan, where all other parameters of interest are freely floated while minimising the Negative Logarithm Likelihood.The constraints are stronger as the cross-sectional terms for the Top-Yukawa interaction are larger than those of the Bottom-Yukawa and Charm-Yukawa interactions.

The parameterisation of the model only included κ_c and κ_b at first, and κ_t was fixed at the Standard Model value. But it could be incorporated into the parameterised model and turned into a freely floating parameter so that another Negative-Log Likelihood scan could be performed.

The impact of a nuisance parameter θ on a parameter of interest κ is estimated as the change in the best-fit value of the parameter of interest between the unconditional fit, and the fit in which the nuisance parameter is fixed to its unconditional best-fit value within the range of one standard deviation. Impact ranking plots are used to evaluate the robustness of the merging process. They vary the nuisance parameters while the κ_b and κ_c are freely floated ATLAS [2023b]. The impact ranking plots are shown in Figures 11 and 12, for the nominal parameterisation and the parameterisation where all the terms independent of κ_b and κ_c are combined into one, respectively. They contain 2 sets of information, the pulls and the effects on κ_b. The effects on κ_b are measured in terms of the standard deviation of maximum Likelihood value of κ_b as the nuisance parameters are varied.

For the merged and unmerged parameterisations, the impact ranking plot can visualise whether merging the uncertainties worked properly, and it seems that combining the terms independent of κ_b and κ_c does not affect the impact ranking plot to a significant degree.

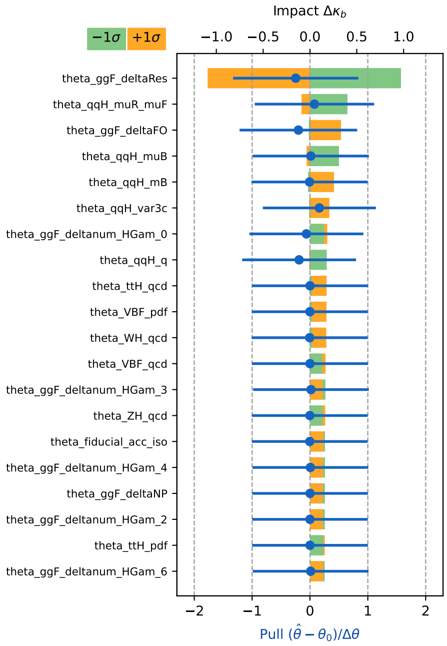

Figure 11: Impact Rankings for κ_b, nominal parameterisation

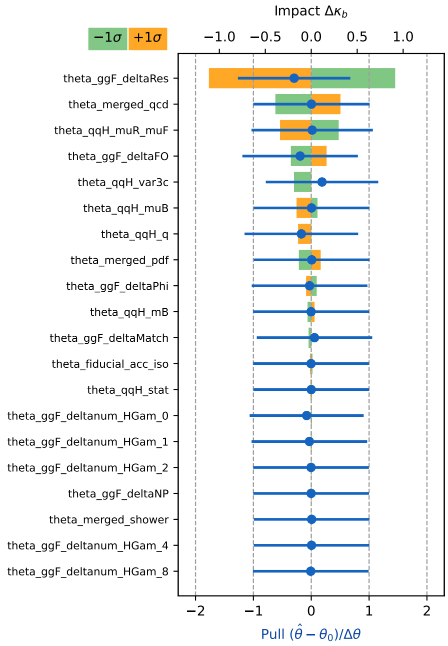

Figure 12: Impact Rankings for κ_b, merged parameterisation

Expected results for Natural-log Likelihood scans can be constructed using Asimov data. This is a Gaussian-distributed toy dataset which is designed to use the covariance matrix of the ATLAS measurements with the mean of the Asimov data being the predicted cross-section Cowan et al. [2011]. Our assumed hypothesis for constructing the Asimov data is the Standard Model predictions. It can give the expected constraints on κ_c, κ_b and κ_t if the Standard Model value of these couplings is assumed to be true. The expected results are shown in Figures 13, 14, and 15.

The Negative Logarithm Likelihood scans that were constructed using the Asimov datasets instead of the ATLAS measurements have stronger constraints for κ_c, κ_b and κ_a than the ones that were constructed using the ATLAS measurements. However, confidence intervals of the Negative Logarithm Likelihood scans constructed using the Asimov datasets are contained inside the confidence intervals of Negative-Log Likelihood scans constructed using the ATLAS measurements, which indicates that the observed data is compatible with the expected data. This means that the parameterised fit demonstrates good behaviour.

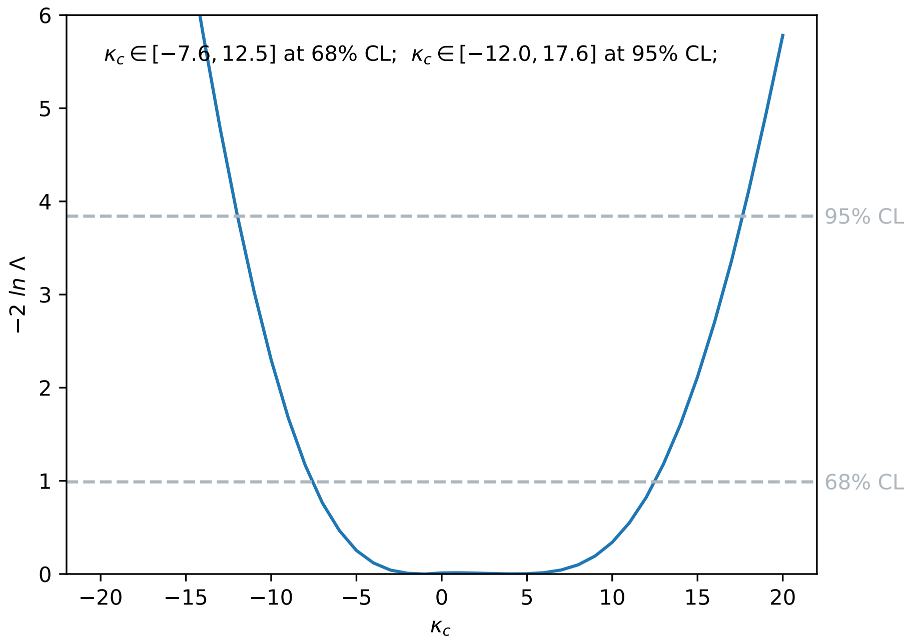

Figure 13: Negative-Log Likelihood scan for κ_b using Asimov data.

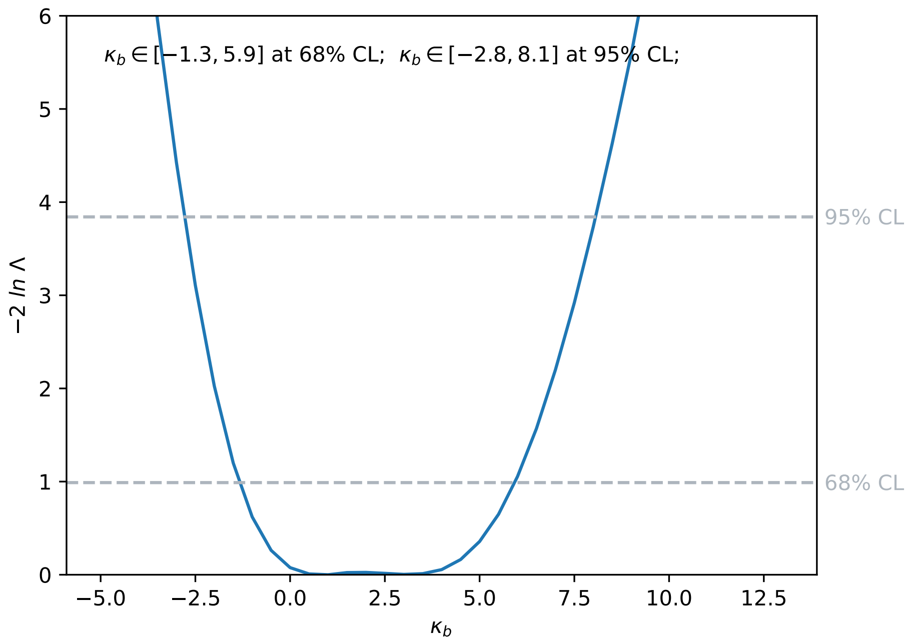

Figure 14: Negative-Log Likelihood scan for κ_b using Asimov data. Notice that there are 2 tiny minima right next to each other, because these minima are a relic of the quadratic terms in the parameterised model.

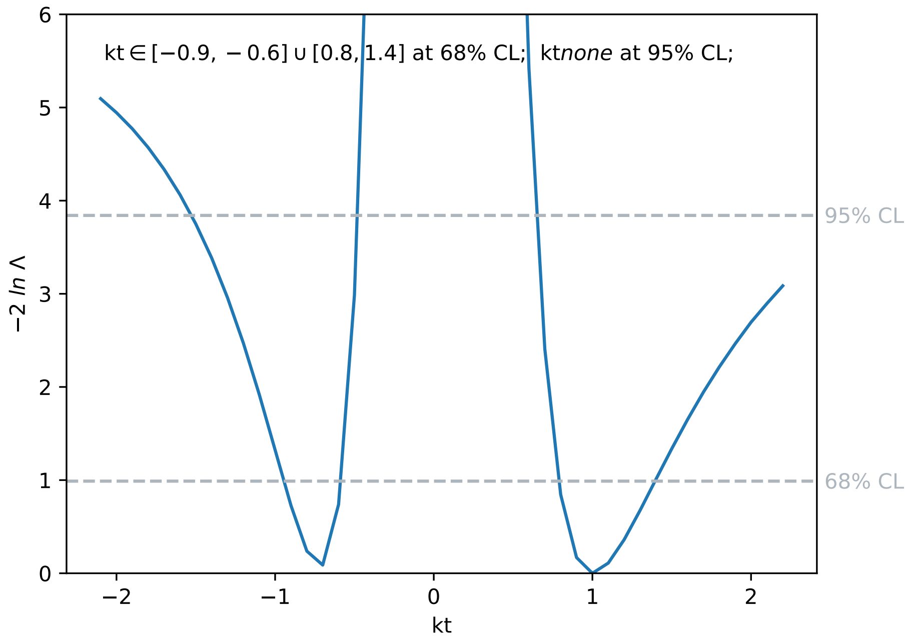

Figure 15: Negative-Log Likelihood scan for κ_t using Asimov data. Because the measured data for κ_t has a stronger constraint than the others and is known to be close to 1, that's why the minimum is around 1.

4 Conclusions

Charm-Yukawa interaction is an intriguing area of investigation because there is the potential for the coupling modifier to deviate from the Standard Model. Currently, the direct $H \to c\bar{c}$ decay has been measured to constrain the Charm-Yukawa coupling modifier even better than the indirect method that is being investigated in this paper, however it is possible to combine the two constraints to make an even stronger constraint.

In future we hope to create a 3-dimensional graph of both κ_b and κ_c with respect to the test statistic, as hopefully this could allow us to see potential correlations between the bottom and charm quark couplings. We also want to constrain κ_b, κ_c and κ_t based on other experimental measurements rather than fixing them to the Standard Model values of 1 or freely floating them.

References

Riccardo Maria Bianchi and ATLAS. ATLAS experiment schematic or layout illustration. General Photo, 2022. URL https://cds.cern.ch/record/2837191.

ATLAS. A detailed map of higgs boson interactions by the atlas experiment ten years after the discovery. *Nature*, 607(7917):52–59, July 2022. ISSN 1476-4687. doi: 10.1038/s41586-022-04893-w. URL http://dx.doi.org/10.1038/s41586-022-04893-w.

Henric Wilkens and ATLAS. The atlas liquid argon calorimeter: An overview. *Journal of Physics: Conference Series*, 160(1):012043, apr 2009. doi: 10.1088/1742-6596/160/1/012043. URL https://dx.doi.org/10.1088/1742-6596/160/1/012043.

ATLAS. Measurement of the higgs boson mass with $h \to \gamma\gamma$ decays in $140fb$ of $\sqrt{s} = 13$ tev pp collisions with the atlas detector. *Physics Letters B*, 847:138315, December 2023a. ISSN 0370-2693. doi: 10.1016/j.physletb.2023.138315. URL http://dx.doi.org/10.1016/j.physletb.2023.138315.

ATLAS. Measurements of W H and Z H Higgs production with decays into bottom quarks and direct constraints on the charm Yukawa coupling with 13 TeV collisions in the ATLAS detector. Technical report, CERN, Geneva, 2024. URL https://cds.cern.ch/record/2905263. All figures including auxiliary figures are available at https://atlas.web.cern.ch/Atlas/GROUPS/PHYSICS/CONFNOTES/ATLAS-CONF-2024-010.

Petar Bokan, Laurelle Maria Veloce, Haider Abidi, Chiara Arcangeletti, Andrea Gabrielli, Paolo Francavilla, Nicolas Morange, Kerstin Tackmann, Sarah Heim, Frued Erik Braren, Gangcheng Lu, Giovanni Marchiori, Daniela Kuchler, Kurt Brendlinger, Nils Gillwald, Martina Laura Ojeda, Roberto Di Nardo, Hongtao Yang, Ahmed Tarek, Marko Stamenkovic, Miha Muskinja, Tao Wang, Yusheng Wu, Heather Gray, and Tristan Arnoldus Du Pree. Combination of the total inclusive and differential Higgs boson cross-sections and interpretations. Technical report, CERN, Geneva, 2022. URL https://cds.cern.ch/record/2804361.

CMS and ATLAS. Combination of measurements of the top quark mass from data collected by the atlas and cms experiments at $\sqrt{s} = 7$ and 8 tev, 2024. URL https://arxiv.org/abs/2402.08713.

R. L. Workman et al. Review of Particle Physics. *PTEP*, 2022:083C01, 2022. doi: 10.1093/ptep/ptac097.

ATLAS. Measurement of the total and differential higgs boson production cross-sections at $\sqrt{s} = 13$ tev with the atlas detector by combining the$h \to zz* \to 4l$ and $h \to \gamma\gamma$ decay channels. *Journal of High Energy Physics*, 2023(5), May 2023b. ISSN 1029-8479. doi: 10.1007/jhep05(2023)028. URL http://dx.doi.org/10.1007/JHEP05(2023)028.

Fred James and Matthias Winkler. *MINUIT User's Guide*, 6 2004.

Glen Cowan, Kyle Cranmer, Eilam Gross, and Ofer Vitells. Asymptotic formulae for likelihood-based tests of new physics. *The European Physical Journal C*, 71(2), February 2011. ISSN 1434-6052. doi: 10.1140/epjc/s10052-011-1554-0. URL http://dx.doi.org/10.1140/epjc/s10052-011-1554-0.

ATLAS. Measurement of the total and differential higgs boson production cross-sections at $\sqrt{s} = 13$ tev with the atlas detector by combining the $h \rightarrow zz^* \rightarrow 4l$ and $h \rightarrow \gamma\gamma$ decay channels. *Journal of High Energy Physics*, 2023(5), May 2023c. ISSN 1029-8479. doi: 10.1007/jhep05(2023)028. URL http://dx.doi.org/10.1007/JHEP05(2023)028.